Photoelectron diffraction study of the Si-rich 3*C*-SiC(001)–(3×2) structure

A. Tejeda,[1,2] D. Dunham,[3,*] F. J. García de Abajo,[4] J. D. Denlinger,[5] E. Rotenberg,[5] E. G. Michel,[1,2] and P. Soukiassian[2,3]
[1]*Departamento de Física de la Materia Condensada and Instituto de Ciencia de Materiales Nicolás Cabrera, Universidad Autónoma, 28049 Madrid, Spain*
[2]*Commissariat à l'Energie Atomique, Laboratoire SIMA associé à l'Université de Paris-Sud/Orsay, DSM-DRECAM-SPCSI, Bâtiment 462, Saclay, 91191 Gif-sur-Yvette Cedex, France*
[3]*Department of Physics, Northern Illinois University, DeKalb, Illinois 60115-2854, USA*
[4]*Centro Mixto CSIC-UPV/EHU and Donostia International Physics Center (DIPC), Apartado 1072, 20080 San Sebastián, Spain*
[5]*Advanced Light Source (ALS), Ernest Orlando Lawrence Berkeley National Laboratory, Berkeley, California 94720, USA*
(Received 22 December 2003; revised manuscript received 22 March 2004; published 27 July 2004)

The structure of the Si-rich 3*C*-SiC(001)–(3×2) surface reconstruction is determined using soft x-ray photoelectron diffraction. Photoelectrons are detected along a full hemispherical sector for different photon energies. A comparison between the experimental data and multiple scattering calculations of the competing models favors a modified version of the two-adlayer asymmetric dimer model. An *R*-factor analysis has been employed to refine this model. We determine the interlayer spacings of the last six atomic layers and find a corrugation of (0.25±0.10) Å for the atoms in the outermost dimer. Atoms in the second layer dimerize as well, forming rows of long and short dimers.

DOI: 10.1103/PhysRevB.70.045317 PACS number(s): 68.35.Bs, 61.14.Qp

I. INTRODUCTION

Silicon carbide is a IV-IV compound wide band-gap semiconductor with applications in high-temperature, high-power, high-voltage, and high-frequency electronic devices and sensors.[1–3] The hexagonal (α) polytypes have the larger band gap (up to 3.3 eV) and are preferred for high temperature/high power devices. The cubic (β, also called 3*C*-SiC to stress the cubic symmetry) polytype (band gap of 2.4 eV) is found to be more suitable for high-frequency devices due to higher carrier mobilities.[1] However, it is only recently that well-defined surfaces of 3*C*-SiC could be obtained. The (001) face has been the most studied so far due to the expected similarity with corresponding elemental group IV semiconductors such as Si or Ge. 3*C*-SiC(001) has more than 10 different surface reconstructions ranging from Si-rich to C-rich surfaces, and it has attracted much attention both in experiment[4–26] and theory.[27–33]

The general form of the surface reconstructions of Si-rich 3*C*-SiC(001) is $[(2m+1)\times 2]$, when m is an integer, when prepared under adequate conditions.[34] The (3×2) structure has the smallest unit cell of the series.[35] These reconstructions have deserved attention during the last few years due to several reasons. First, these surface phases are Si-terminated. Due to the difference of lattice parameters between Si and SiC, their last atomic layers are an example of a two-dimensional Si crystal under compression. Thus the different layers are subject to significant deformations, but their atomic arrangement is not known in detail. Second, the high-m reconstructions are constituted by long atomic chains, forming in some cases true nanowires on the surface.[36–38] Finally, these phases are strongly reactive towards oxygen[14] or hydrogen,[26] recently found to induce surface metallization of the (3×2) reconstruction.[26] These very interesting and unprecedented properties are driving forces towards the knowledge and the understanding of the surface and subsurface atomic structure of the (3×2) phase.

After the pioneering work of Dayan[6,7] using low-energy electron diffraction (LEED), different well-established surface sensitive techniques have been applied to investigate the nature of the (3×2) reconstruction.[9–11] More recently, advanced techniques like core level and valence band photoemission[16–18] and scanning tunneling microscopy (STM)[35] have been also used to analyze this surface. However, contradictory models are found in the literature for its atomic structure. This is due to the fact that there is no direct structural information, besides the lateral atomic distribution provided by STM,[35] with the exception of a recent grazing incidence x-ray diffraction (GIXRD) study.[39] Thus several different atomic models can be found in the literature for this reconstruction (see Fig. 1). In ADRM (alternate dimer row model) (2×3),[30] the long side of the unit cell is parallel to the $[\bar{1}10]$ direction. There is one dimer per unit cell over a full Si layer and dimers are perpendicular to the rows. In ADRM (3×2),[35] the long sides of the unit cell are parallel to the $[110]$ direction. There is one dimer per unit cell over an unknown layer. Dimers are perpendicular to the rows. SDRM (single dimer row model)[9] has one dimer per unit cell over a full Si layer. Dimers are parallel to the rows. SDDRM (symmetric double dimer row model) contains two symmetric dimers per unit cell over a full Si layer.[7] ZZAFM-DDRM (zigzag antiferromagnetic DDRM) has two asymmetric dimers per unit cell disposed in zigzag over a full Si layer. Dimers are buckled in the same sense, in such a way that adjacent atoms of neighboring dimers have different heights. ZZFM-DDRM (zigzag ferromagnetic DDRM) has two asymmetric dimers per unit cell disposed in zigzag over a full Si layer.[31] Atoms of different heights of consecutive dimers are adjacent.[31] LAFM-DDRM (layered antiferromagnetic DDRM) includes two side-by-side asymmetric dimers per unit cell over a full Si layer.[31] Dimers are tilted in opposite senses. LFM-DDRM (layered ferromagnetic DDRM) has two side-by-side asymmetric dimers per unit cell over a

 ©2004 The American Physical Society

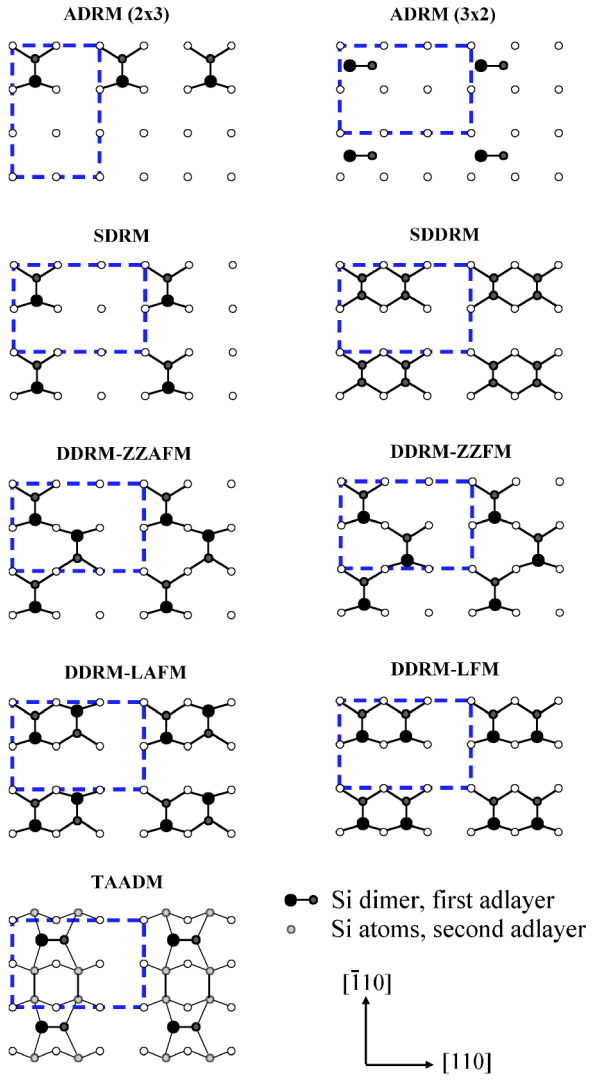

FIG. 1. (Color online) Schematic representation of the atomic positions in the different models found in the literature for the (3×2) reconstruction of 3*C*-SiC(001). See text for details and model description.

full Si layer.[31] Dimers are tilted in the same sense. In TAADM (two adlayer asymmetric dimer model)[31] the last layer (1/3 monolayer, ML) is formed by one dimer per unit cell. This layer lies on top of a layer with two dimers per unit cell (2/3 ML). The third layer is complete (1 ML). Depending on the element forming this layer (Si or C), we consider TAADM-Si or TAADM-C models. Finally, the alternating short and long dimer model (ALSD)[39] is a modified version of the TAADM-Si (not shown in Fig. 1, see also below).

In this paper we investigate the structure of the 3*C*-SiC(001)$-(3\times2)$ surface reconstruction using the information provided by soft x-ray photoelectron diffraction (PED).[40,41] This technique has been successfully applied to determine the structure of many semiconductor and metal/semiconductor surfaces.[42–52] At variance with GIXRD or LEED, the PED technique allows one to obtain atom-specific structural information. This is especially interesting in the case of a compound semiconductor because photoelectrons from both Si and C atoms can be detected and used for the structural determination (see Fig. 2). It is also important in the case of a complex reconstruction like the (3×2) phase that involves several Si layers. Furthermore, the PED technique does not need long range order in the surface, but only short range order. The PED technique has not yet been applied to the 3*C*-SiC(001), with the exception of a study on the C-terminated $c(2\times2)$ phase[53] made in the backscattering mode. In this paper we use two ranges of photon energies (150–210 eV and 1253.6 eV) to investigate both the atomic structure of the (3×2) surface reconstruction and the interlayer spacing of the last bulk atomic layers. We obtain a large data set ($\sim$350 experimental points) that is analyzed using an exact multiple scattering formalism using spherical waves. This allows us to discern easily the atomic model of the reconstruction and to refine it with high accuracy. We conclude that the (3×2) reconstruction is well described by the recently proposed alternate long and short dimer model (ALSD),[39] a modification of the TAADM-Si model.[31] The different sensitivity of PED as compared to GIXRD allows us to provide new detailed structural information on several aspects of the surface reconstruction.

II. DATA ANALYSIS AND EXPERIMENT

The outgoing electron wave field originating in the excitation of a core level in a photoemission experiment is diffracted by atoms in the vicinity of the emitter, so that the far field distribution of photoelectrons carries information on the relative positions of neighboring atoms with respect to the emitting atom. This phenomenon is used in the PED technique to gain insight into atomic surface structures. We refer the reader to Refs. 40 and 41 for more details. In this work, the experimental intensity modulations were compared with the results of a suitable scattering formalism that simulates the measured PED by modeling the structure of the last atomic layers.[54,55] The EDAC code was used for the simulations,[55] conveniently adapted to the geometry of our experimental setup. The code is based upon a multiple-scattering cluster approach, where the surface is represented by a sufficiently large number of atoms surrounding the emitter (over 2000 in the present case). Multiple scattering of the photoelectron in its way towards the detector is solved using a stable iterative technique until convergence is achieved (here, after 11 iterations) with full inclusion of curved wave effects and no further approximations besides those inherent of a muffin-tin construction. The converged calculated results were used to discern the correct surface structure of Si-rich 3*C*-SiC(001)$-(3\times2)$, obtained from a systematic search between the models proposed in the literature.[6,7,9,11,30,31,35,39]

We use a cluster of more than 2200 atoms, with a mean-free-path dependent attenuation of the electron yield.[56] The inner potential and the surface position are considered a parameter that is fitted to optimize the agreement with the experiment. We use isotropic Debye-Waller factors to account for the thermal vibrations. No difference between surface and bulk atoms is considered. Simulated PED patterns are generated with emitters at symmetry-inequivalent sites in the first to seventh topmost surface layers. Two-domain samples

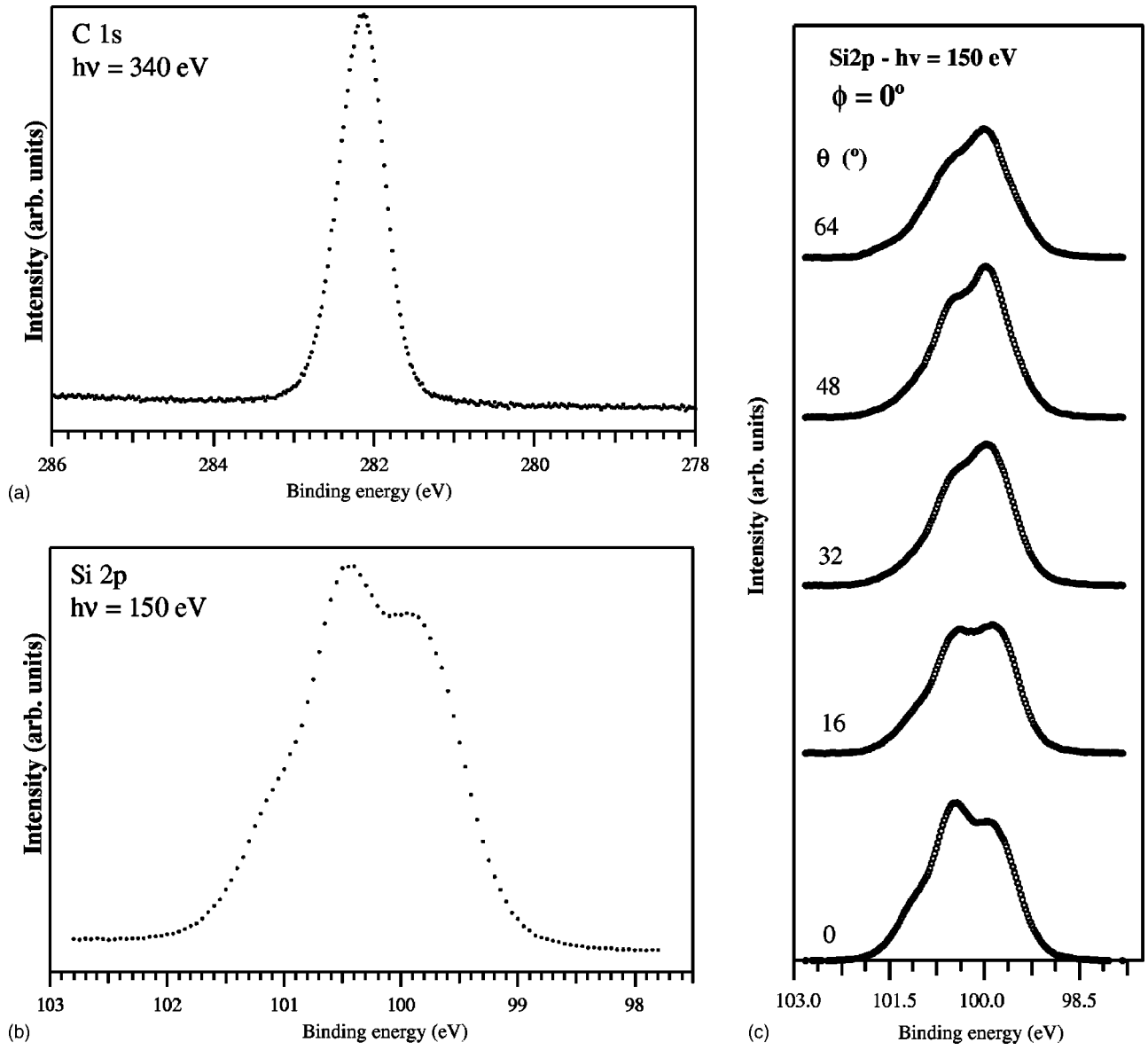

FIG. 2. (a) C 1*s* core level for $h\nu=340$ eV and normal emission. (b) Si 2*p* core level $h\nu=150$ eV and normal emission. (c) Si 2*p* core levels as a function of emission angle θ for $\phi=0$. Note the changes in intensity and line shape.

(corresponding to 180° rotation) are considered in the simulation.[58] The Si and C muffin-tin scattering phase shifts are used. The quality of the surface model is judged on the basis of the agreement between theory and experiment that is measured by the figure of merit R (R_1-factor of Saiki *et al.*[59,60]), defined as

$$R = \frac{\sum_n |\chi^{\ddagger}_{\mathrm{exp}}(n) - \chi^{\ddagger}_{\mathrm{th}}|}{\sum_n |\chi^{\ddagger}_{\mathrm{exp}}(n)|} \qquad (1)$$

where $\chi^{\ddagger}_{\mathrm{exp}}$ and $\chi^{\ddagger}_{\mathrm{th}}$ are the experimental and theoretical normalized anisotropies, respectively,[59,60] and n corresponds to the channel of the azimuthal scan. This is a very useful factor as it avoids excess influence of experimental noise at high polar angles. R also allows one to know the sensitivity of the different parameters and to refine the atomic structure. The surface model is modified until a good value of $R(\lesssim 0.04)$ is reached.

The experiments are performed in an ultrahigh vacuum chamber equipped with an angle resolving hemispherical analyzer and a manipulator that allows sample rotation, receiving synchrotron light from the 7.0.1 beamline of the Advanced Light Source. Since the PED scans are made by rotating the sample, the angle between incident light and electron analyzer is kept constant during the measurements. For each polar emission angle, a series of Si 2*p* ($h\nu=150$, 175, and 210 eV) and C 1*s* ($h\nu=340$ and 365 eV) spectra corresponding to different azimuthal angles is recorded. Additional high energy data for both core levels are obtained using a Mg K_α ($h\nu=1253.6$ eV) x-ray source. The symmetry of the system is checked with several 180° azimuthal scans. The sample is oriented by LEED and the orientation is refined *in situ* using photoelectron diffraction scans. The [110]

direction is taken as the reference for azimuthal emission angles and the normal emission for polar emission angles. A series of azimuthal scans (ϕ, azimuthal emission angle) is obtained by rotating the sample around its normal 100° for low energy incident photons and 120° for Si 2*p* Mg K_α data. The polar emission angle θ is varied between 0° and 72° (8° steps for low photon energy and 4.5° steps for high photon energy data). In each of the Si 2*p* low energy series, 105 experimental points are taken. For C 1*s* and for the high energy data, 320 points are taken. The absolute angular precision is 0.5° for θ and 1° for ϕ.

We use 1 μm SiC thin films prepared at LETI (CEA-Technologies Avancées) by C_3H_8 and SiH_4 chemical vapor deposition (CVD) growth on Si(100) wafers with a miscut angle of 4° to prevent the formation of 90° rotated domains. The high-quality Si-rich 3*C*-SiC(001)$-(3\times2)$ surface reconstruction is obtained by thermal cleaning, followed by Si evaporation at room temperature to restore the Si stoichiometry and flashing the crystal to 1000 °C, as explained in Ref. 35.

III. RESULTS

As first step, we monitor the Si 2*p* peak for $h\nu = 1253.6$ eV. Since the kinetic energy of both core levels is several hundreds of eV, forward scattering dominates the PED process.[40,41] In this kinetic energy range and due to the larger electron mean free path, data are more sensitive to bulk atomic positions, i.e., to atomic layers well below those affected by the surface reconstruction [see Fig. 3(a)]. The mean free path calculated from the TPP-2 approximation is 19 Å.[57] A good agreement between theory and experiment is reached with only minor distortions of bulk atomic positions. The cluster employed in the simulations is of TAADM type, but the results are almost independent of the surface reconstruction for this photon energy because the surface layer represents a minor contribution to the total signal. Figure 3(b) shows the *R*-factor variation for Si 2*p* data with respect to its minimum ($R_{\min}$) as a function of the factor $f = c/4.36$, which corrects the lattice parameter *c*. *f* is varied between 0.75 and 1.25 in 0.05 steps. The *R*-factor analysis shows that $c = (4.36 \pm 0.10)$ Å, consistent with the expected bulk lattice parameter (4.36 Å). A comparison between theory and experiment for a polar cut along the $[\bar{1}10]$ direction is also shown in Fig. 3(d) ($f = 1.00$). Maxima, minima, and the shape of the experimental curve are well reproduced by the simulation.[61] The high kinetic energy regime allows also to study subsurface layers independently of the surface reconstruction [see Fig. 3(c)]. After optimizing the atomic positions, we find that the interlayer spacings are Δz(III-IV) $= (0.89 \pm 0.05)$ Å, Δz(IV-V) $= (1.00 \pm 0.05)$ Å, and Δz(V-VI) $= (1.09 \pm 0.05)$ Å, that is equal to the bulk value.

As a second step, the bulk atomic positions so determined are used to construct a series of clusters that reproduce the different structural models shown in Fig. 1. The atomic positions of the surface layers are taken from the values proposed in the literature for each model. These clusters are used to model the experimental anisotropy curves. Low-energy data are sensitive to the structure of the topmost surface layers, and thus they are adequate to distinguish between the different models.[62] A perfect agreement between experiment and theoretical simulation is not expected at this level because this would require a detailed model refinement.

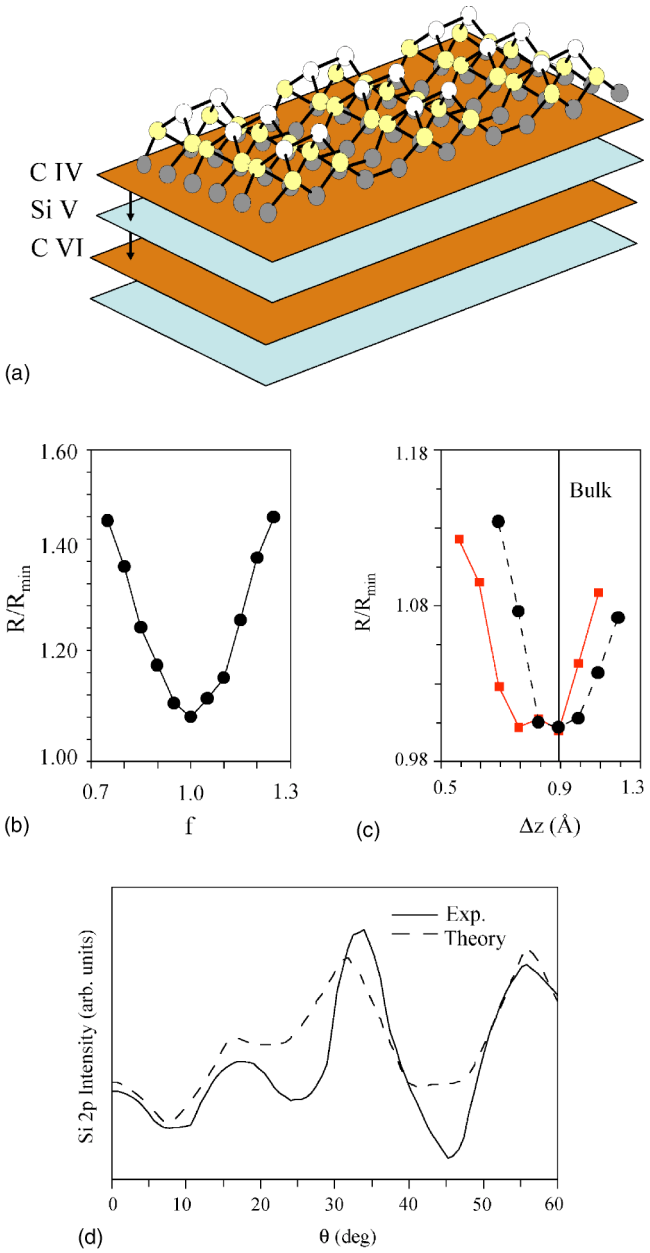

FIG. 3. (Color online) High kinetic energy studies. (a) Schematic representation of the layers. A TAADM model has been considered, but for these experimental conditions there is a negligible contribution of the surface signal. (b) *R*-factor relative to its minimum as a function of the factor $f = c/4.36$. (c) *R*-factor relative to its minimum as a function of the interlayer spacing between layers IV and V (red squares) and layers V and VI (circles). The vertical line shows the bulk spacing between consecutive layers in 3*C*-SiC(001). While there is a small relaxation in the spacing between layers IV and V, the spacing between layers V and VI is identical to the bulk value. (d) Polar scan along the $[\bar{1}10]$ direction in the cluster corresponding to the minimum in (a) and theoretical simulation.

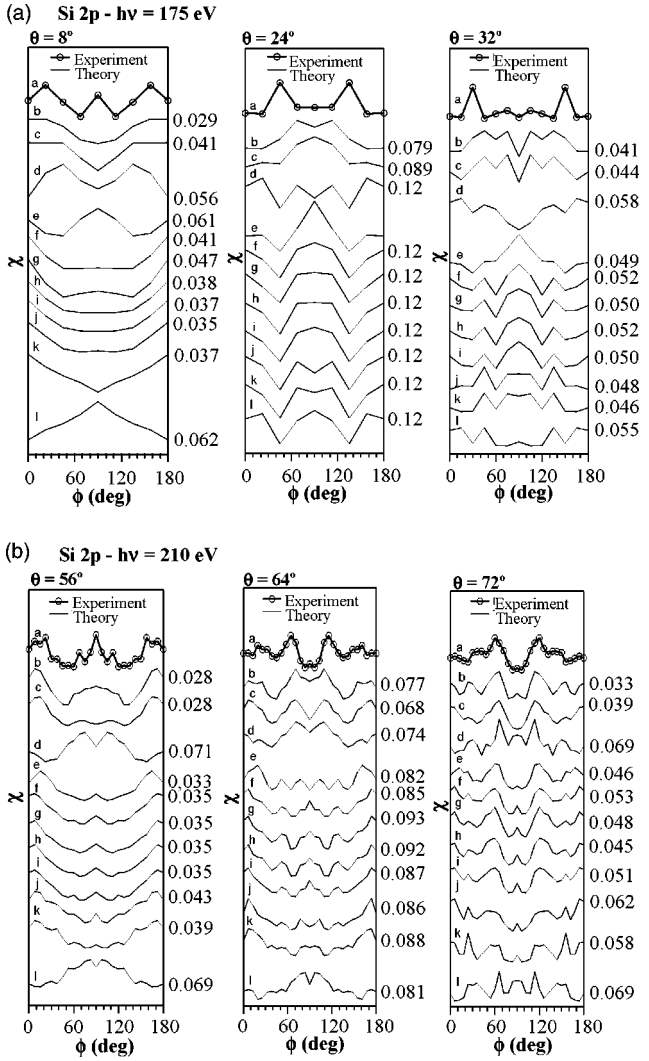

FIG. 4. Model discrimination. Panels (a) (175 eV) and (b) (210 eV): comparison between the experimental azimuthal anisotropy curve of Si 2*p* photoemission peak (*a*, circles) and the theoretical simulation for the different models (lines). Polar emission angles and energies have been selected to highlight the differences between the proposed structural models. The simulated models are: b: ALSD, c: TAADM-Si, d: TAADM-C, e: SDDRM, f: DDRM-ZZFM, g: DDRM-ZZAFM, h: DDRM-LFM, i: DDRM-LAFM, j: SDRM, k: ADRM, (2×3) and l: ADRM (3×2) (see text for details). The right columns show the *R* factor value for the corresponding model, calculated according to Eq. (1).

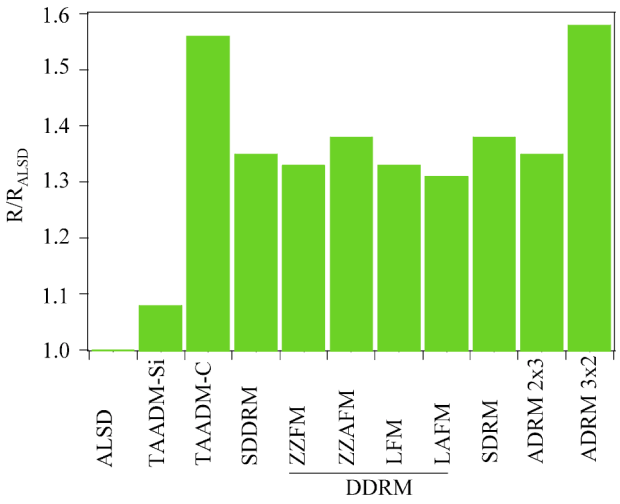

FIG. 5. (Color online) Comparison of the mean *R*-factor of the different models relative to that of the ALSD model (R_{ALSD}). The mean *R*-factors shown are an average of all azimuthal anisotropy curves.

However, if the agreement between model and experiment is poor, the model can be safely discarded without further tests because minor modifications of the atomic positions are not able in general to revert the situation to a good agreement. Mostly Si 2*p* data were used during the refinement because they are more sensitive to structural changes than C 1*s* data. Figure 4 shows a comparison between the experimental azimuthal anisotropy curves at three different polar angles for the photon energies of 175 and 210 eV, and the predictions of the different models. We select in Fig. 3 those polar angles that enhance the differences between the models. A visual inspection of Fig. 4 reveals that only ALSD-TAADM models are able to reproduce the general features of all the experimental curves (curves a). For $h\nu=175$ eV and $(\theta,\phi)=(24°,180°)$ the experimental azimuthal anisotropy curve exhibits a minimum that is only reproduced by the ALSD model (curve b). For $h\nu=175$ eV and $\theta=32°$ the TAADM models (curves b–d) and the ADRM (2×3) (curve k) are the only models able to reproduce the number and approximate positions of experimental peaks. In particular, DDRM models (curves e–i) show a maximum at $\phi=90°$ that is not present in the experimental curve. For $h\nu=210$ eV, the ALSD model reproduces quite well the general features of the experimental curve. A more quantitative comparison between the models can be made by means of an *R*-factor analysis (right columns in Fig. 4). The only curve that has a smaller *R*-factor than the ALSD model is curve c (TAADM-C) for $h\nu=210$ eV and $\theta=64°$, panel (b), but it is not the case for all the other panels. All models exhibit in average an *R*-factor higher than that of the ALSD model by at least 30%. Furthermore, a mean *R*-factor can be calculated for each of the models so compared. The mean *R*-factor includes all the experimental points measured. The much better agreement of TAADM Si-ALSD models is clear from Fig. 5. *R* is also at least 30% higher in the rest of the models than in ALSD. The models that are less favored are TAADM-C and ADRM (3×2). The ALSD model is favored in a wide range of azimuthal and polar angles, and for two different photon energies. This analysis allows one to discard all the models with the highest *R*-factor. Thus in the following we work on the basis of TAADM-Si and ALSD models only.

Once the overall features of the surface atomic structure (atomic model) are clear, the third step is the refinement of the structure to obtain the best possible agreement with the experimental data. To this end, the surface structural parameters are systematically modified until an absolute minimum in the *R*-factor is found. The positions of all atoms in the three first layers of the cluster are changed during the structure refinement process, without symmetry breaking. The number of varied parameters was 14, including 11 structural

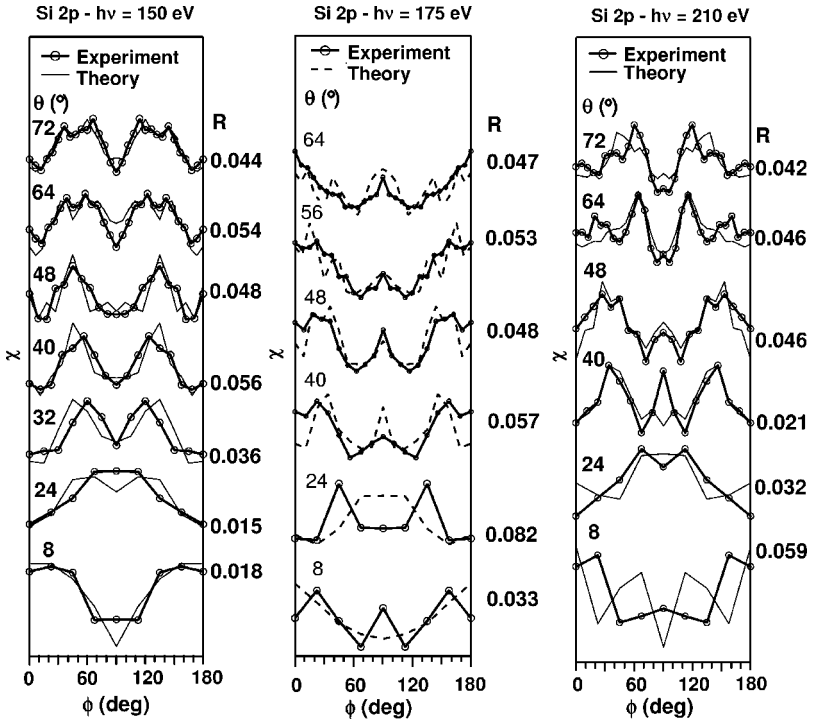

FIG. 6. Comparison between Si 2*p* experimental (circles) and simulated azimuthal anisotropy curves (thin line) for the refined model. The photon energies are $h\nu = 150$ eV (left), 175 eV (center), and 210 eV (right). Selected curves corresponding to different polar angles are shown in each panel.

parameters [$x_1, z_1, x_2, z_2, x_3, y_3, z_3, x_4, y_4, z_4$, and the vertical coordinate of the third layer $z(III)$] and three nonstructural parameters (inner potential, surface position, and mean free path[56]). The total number of experimental points was 375. This gives a ratio of ~27 experimental points per parameter. In order to keep reasonable computing times, we consider in the refinement process the two extreme photon energies with surface sensitivity of the Si 2*p* data set (150 and 210 eV). We reach a minimum of *R*-factor for this model of 0.039, which corresponds to an improvement of almost 70% with respect to the initial value.[63] Figure 6 shows a selection of the corresponding Si 2*p* experimental and theoretical anisotropy curves for $h\nu = 150$, 175, and 210 eV for the refined model. The visual agreement between the experiment and simulation is very good for the different photon energies used and for a wide range of polar and azimuthal angles. Azimuthal anisotropy curves for C 1*s* and the corresponding simulations for the same atomic structure are shown in Fig. 7. An excellent agreement is also found in this case.

An example of the refinement process is shown in Figs. 8 and 9, where the *R* factor value is represented as a function of different structural parameters. The structure found is shown schematically in Fig. 10. Figure 8 shows an *R*-factor map as a function of the vertical coordinates of the atoms of the topmost dimer (atoms 1 and 2 in Fig. 10). The minimum found corresponds to an asymmetric dimer configuration, with a difference of height of (0.25 ± 0.10) Å. Each atom of the dimer is bonded to two other Si atoms which dimerize as well. Figure 9 shows the *R*-factor as a function of the bond lengths of atoms in the second layer. Both minima correspond to the same bond length between atoms 3 and 5, $d(3-5) = (2.40 \pm 0.10)$ Å. However, they provide two different values for $d(4-6)$. The first minimum (~1.5 Å) corresponds to a bond length that is close to the Si covalent radius (1.17 Å). Thus it can be discarded. The other minimum corresponds to a bond length of ~1.8 Å, which is 20% smaller than a Si–Si bulk distance. In view of the lack of an absolute minimum and the fact that the contour lines are wider, this value is affected by a larger error. The final value is $d(4-6) = (1.83 \pm 0.20)$ Å. The larger error bar is not due to the quality or size of the data set, but rather to the relatively higher insensitivity of the azimuthal anisotropy curves to this parameter. However, we can safely conclude that the bond length of the second layer dimers varies depending on whether they are bonded to the upper [(2.40 ± 0.10) Å] or lower atom [(1.83 ± 0.20) Å] of the first layer dimers.

Two pairs of atoms per unit cell in the third layer (7–9 and 10–12) dimerize as well. The bond length of these dimers is (2.43 ± 0.10) Å. Therefore the dimerization in the last three layers of the material reduces from six to two the number of dangling bonds per unit cell. Besides the values of the interlayer distance for layers III to VI mentioned above, we find that for layers I–III, $\Delta z(\text{I-II}) = (1.26 \pm 0.05)$ Å and $\Delta z(\text{II-III}) = (1.43 \pm 0.05)$ Å. The structural parameters found are summarized in Tables I and II. Table I gives the coordinates of the atoms in the last layers while Table II provides structural parameters like layer spacings and bond lengths.[65]

IV. DISCUSSION

The good agreement found between the theoretical simulations and the experiment allows us to discard DDRM, SDRM, and ADRM models. Only a variation of the TAADM model can reproduce the data. We summarize now the main features of the atomic structure found, and in the following paragraphs we compare this model with the atomic structure obtained from GIXRD data[39] and the predictions of *ab initio* calculations.[31] If we consider a Si-terminated bulk 3*C*-SiC(001) crystal, the ALSD or TAADM models consist of

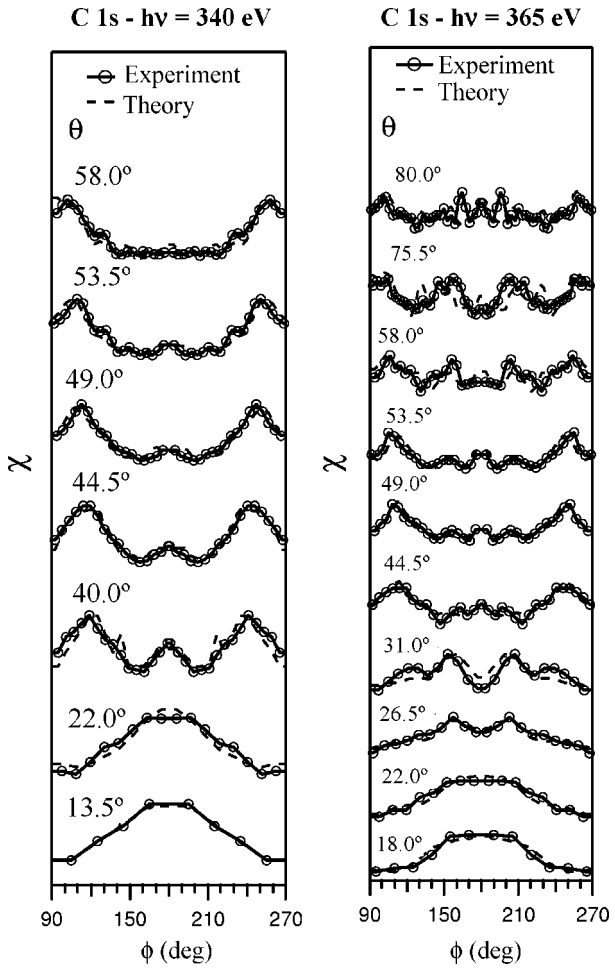

FIG. 7. Comparison between experimental (circles) and simulated azimuthal anisotropy curves (thin lines) for C 1*s* for the refined model. The photon energies are $h\nu = 340$ eV (left) and 365 eV (right). Selected curves corresponding to different polar angles are shown in each panel.

two additional Si layers on top (layer I, with 1/3 ML of Si atoms, and layer II with 2/3 ML of Si atoms, both shown in Fig. 10). The topmost substrate Si layer (layer III in Fig. 10) is also modified due to the reconstruction. In order to understand its features, we start by examining the vertical distances between layers (see Table II). Δz(V-VI) is equal to the bulk interlayer spacing, while Δz(IV-V) is slightly shorter (1.00 Å). Δz(III-IV) is even smaller (0.89 Å). The distance between the two additional Si layers is Δz(I-II) = 1.26 Å and Δz(II-III) = 1.43 Å. These two values are close to the Si(100) interlayer distance (1.36 Å). The connection between the top reconstructed layers and the SiC substrate is made between layers III and IV. Layer III is formed by Si atoms forming rows of dimers (between atoms 7-9 and 10-12). There is no vertical corrugation within layer III. Layer IV is formed by C atoms already at bulk positions, but the III-IV interlayer spacing is contracted with respect to the bulk value. The bulk interlayer spacing value is only reached between layers V and VI. Thus the transition between the SiC and Si interlayer spacings takes place very fast, in spite of the fact that the lateral lattice distances (*X* or *Y* direction in Fig. 10) are fixed by the substrate to the SiC value (3.08 Å). This means that Si layers II and I are subject to a strong lateral stress, equivalent to a compression, due to the large (~20%) difference in lattice parameters between Si (5.43 Å) and SiC (4.36 Å). These two layers are stabilized through a combination of factors. First, the two layers are relatively open because their coverages are smaller than the nominal value of 1 ML. This facilitates a partial relaxation of the layer. Second, due to the atomic structure of the reconstruction, all Si–Si bonds are fairly close to the Si bulk value (2.34 Å). If we examine the Si–Si bond lengths between layers II (atoms 3–6) and III (atoms 7–12), see Table II, we find values around 2.3 Å, i.e., slightly shorter than the Si bulk value, while the II-III interlayer distance is slightly longer (1.4 Å) than the Si bulk value. The small lateral distances of layer III facilitate that atoms in layer II saturate the dangling bonds in layer III. A combination of shorter bond lengths and longer interlayer distance makes layer II atoms close to Si bulk values, which certainly reduces the stress. In particular, the lateral compression on layer II and the reduced coverage determine a value of Δ(II-III) longer than in Si(100).

The (3×2) structure is terminated by layer I, formed by asymmetric Si dimers. We get an intradimer bond length of (2.54 ± 0.20)Å and a height difference of (0.25 ± 0.10)Å. These values correspond to a dimer angle of $(5.5\pm3)°$. They can be compared to equivalent values from Si(100) dimers: (2.37 ± 0.06)Å and $(20\pm3)°$ (from Ref. 66) and 2.25 Å and $(19.0\pm0.5)°$ (from Ref. 46). Due to the different atomic arrangement of the reconstruction, Si atoms in layer II can relax laterally much more than in Si(100). Thus a longer dimer bond length with smaller tilt angle is found. The dimer height difference gives rise to two different effects in layer II. First, there is a small vertical corrugation of (0.03 ± 0.10) Å within layer II, from values in Tables I and II [as in Si(100) and Ge(100)]. Second, the lateral relaxation of layer II, with alternating short and long dimers, explains a unique feature of the 3*C*-SiC(001)$-(3\times2)$ reconstruction: in a domain of the (3×2) reconstruction all dimers are tilted in the direction perpendicular to the dimer rows. Moreover, they do not exhibit any alternateness in the tilt angle along the dimer rows. This is different from reconstructions of other group IV semiconductors, like Si or Ge. The structure found in this work allows one to trace back this property to the peculiar structure of layer II. The Si–Si bond lengths between layer I (atoms 1 and 2) and layer II (atoms 3–6) are $d(1-3)$, $d(1-5)=(2.34\pm0.10)$ Å (upper dimer atom 1) and $d(2-4)$, $d(2-6)=(2.59\pm0.10)$ Å (lower dimer atom 2). Note that the relatively large value of $d(2-4)$, $d(2-6)$ is related to the short value of $d(6-4)$.

The main features of the reconstruction are found consistent with STM[35] and GIXRD[39] measurements, and with *ab initio* calculations.[31] The main differences with GIXRD can be summarized as follows (see Table II). GIXRD finds a longer value of the bond length for the topmost dimers that are also less asymmetric. This is probably due to the restricted in *plane* data set in GIXRD data due to experimental limitations.[39] On the other hand, while $d(3-5)$ is close to the GIXRD value, the PED value for $d(6-4)$ is significantly shorter. This discrepancy can be attributed in this case to a

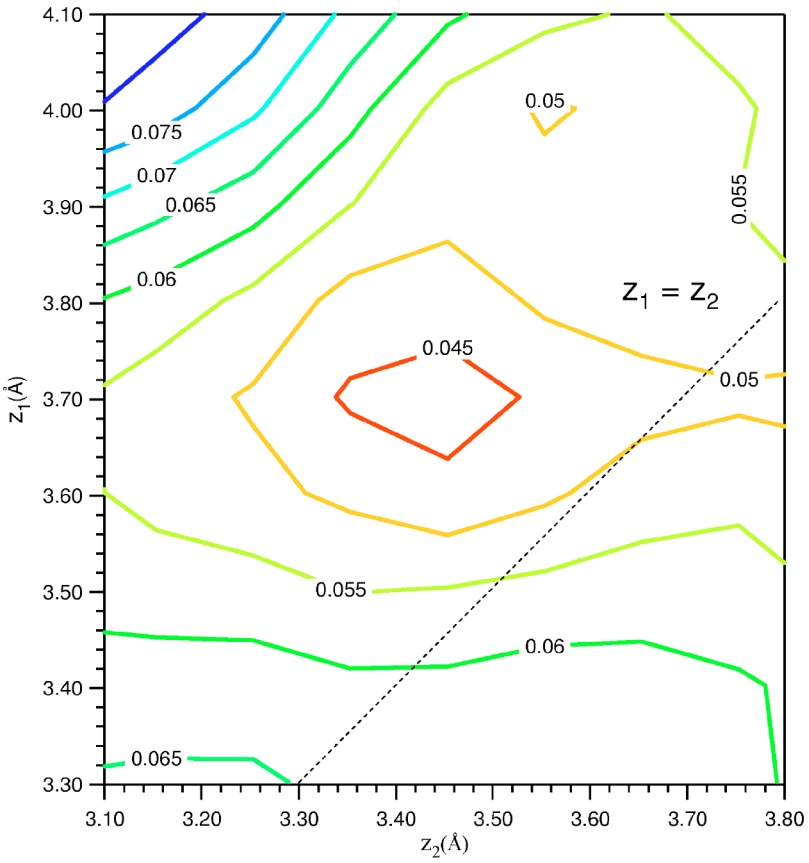

FIG. 8. (Color online) *R*-factor contour plot in the vicinity of the optimal atomic structure. z_1 and z_2 are the vertical coordinates of the last-layer dimer atoms (see Fig. 10). The origin of vertical coordinates ($z=0$) is located at the C atoms of layer IV (see Fig. 3). The dotted line corresponds to a symmetric dimer configuration. The minimum is reached for an asymmetric dimer with $\Delta z = (0.25 \pm 0.10)$Å.

larger error in the PED value. All other values are in very good agreement in both cases. Our high kinetic energy studies allow us to determine the interlayer distances down to layer VI. We also report different values for the two top interlayer distances, at variance with GIXRD.

The *ab initio* calculations from Ref. 31 qualitatively predict well most of the features found both in this study and

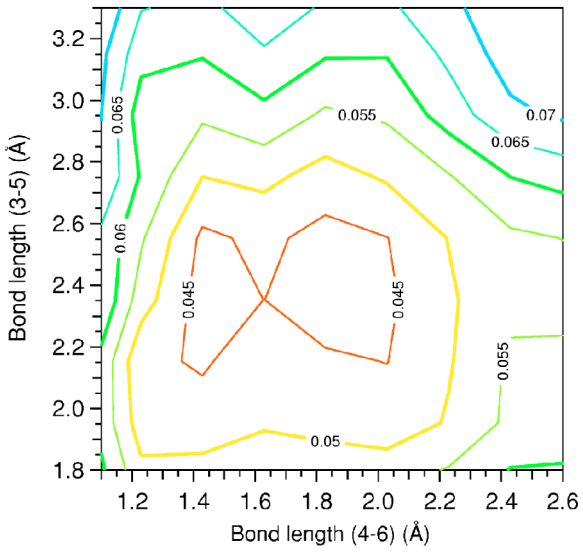

FIG. 9. (Color online) *R*-factor contour plot in the vicinity of the optimal atomic structure. Atoms 3–6 form the second layer dimers (see Fig. 10). Two minima appear for the (4–6) bond length. The shorter value (~1.5 Å) can be discarded because it would correspond to an unphysical Si–Si bond length. The final bond lengths are $d(3-5)=(2.40\pm0.10)$Å and $d(4-6)=(1.83\pm0.20)$Å.

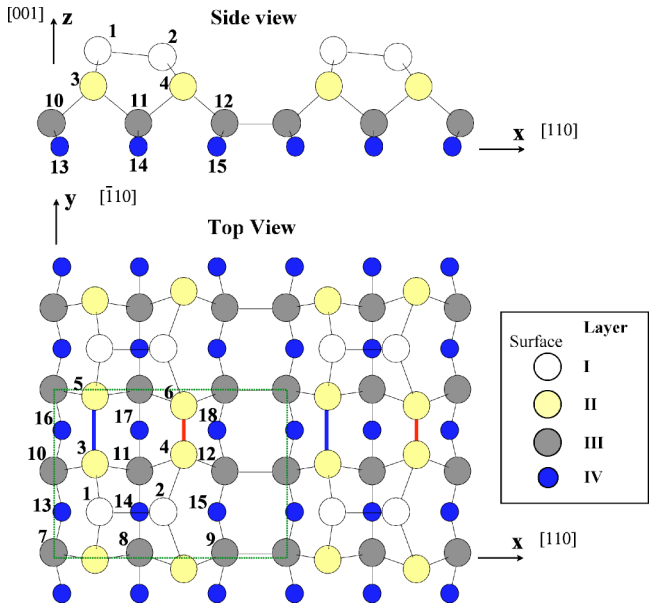

FIG. 10. (Color online) Alternated long and short dimer model. Different views of the model found with atoms in the optimal atomic positions. Si atoms are shown as white (first layer), yellow (second layer), or gray (third layer). Blue C atoms lie in the fourth layer. In the second layer, there are alternately long (5-3, red) and short (6-4, blue) bonds.

TABLE I. Atomic positions of $3C$-SiC(001)$-(3\times2)$. Result from *R*-factor minimization. Roman numbers identify the different atomic layers. All numbers and axis are referred to in Fig. 10. Precision is ±0.05 Å.

Atom	Layer	Element	x(Å)	y(Å)	z(Å)	Atom	Layer	Element	x(Å)	y(Å)	z(Å)
1	I	Si	1.50	1.54	3.70	10	III	Si	−0.33	3.08	0.89
2	I	Si	4.03	1.54	3.45	11	III	Si	3.08	3.08	0.89
3	II	Si	1.32	3.43	2.33	12	III	Si	6.49	3.08	0.89
4	II	Si	4.85	3.71	2.30	13	IV	C	0.00	1.54	0.00
5	II	Si	1.32	5.83	2.33	14	IV	C	3.08	1.54	0.00
6	II	Si	4.85	5.54	2.30	15	IV	C	6.17	1.54	0.00
7	III	Si	−0.33	0.00	0.89	16	IV	C	0.00	4.62	0.00
8	III	Si	3.08	0.00	0.89	17	IV	C	3.08	4.62	0.00
9	III	Si	6.49	0.00	0.89	18	IV	C	6.17	4.62	0.00

with GIXRD.[39] The main differences are the smaller asymmetry of top layer dimers and the existence of alternatively long (3-5) and short (6-4) dimers in the second plane that were not predicted in the *ab initio* calculations.[31]

Our above PED results favor an ALSD-TAADM structural model picture of the $3C$-SiC(001)$-(3\times2)$ surface reconstruction, in excellent agreement with a recent GIXRD investigation.[39] However, one should mention that our model is clearly inconsistent with a reported (3×2) to (3×1) $3C$-SiC(001) surface transformation upon atomic hydrogen exposures.[25] Indeed, in the latter investigation, the orientation of the topmost dimers is probed by LEED claiming such a (3×2) to (3×1) phase transition that seems to take place upon atomic hydrogen exposures.[25] First, one has to remember that room temperature atomic H-exposures on Si surfaces have been shown to result in etching, with Si monohydride and dihydride formation,[67] which would result here in the loss of the $\times2$ LEED reflection. Actually, this (3×1) transition has been assigned by the authors of Ref. 25 to Si−Si dimers breaking, which implies that the dimers are parallel to the $\times2$ periodicity (which is not the case, as shown here, and previously also by STM[35] and GIXRD[39]). Recent real-space atom-resolved STM measurements performed by tunneling into the empty electronic states before and after atomic hydrogen exposure on the surface kept at $T=300\,^{\circ}$C shows reactive sites made of bright double spots of equal intensity.[26] This indicates that the reacted topmost dimers become symmetric upon H-decorating the Si dangling bonds, which

TABLE II. Comparison between the structural parameters of $3C$-SiC(001)$-(3\times2)$ from our PED study, GIXRD studies (Ref. 39), and *ab initio* calculation (Ref. 31). d denotes bond lengths, Δx and Δz denote distances along X and Z directions (all in Å). Atom and layer numbers and directions are referred to in Fig. 10.

Parameter	PED	GIXRD (Ref. 39)	Theory (Ref. 31)
$d(1-2)$	(2.54±0.10)	(2.78±0.03)	2.24
$\Delta z(1-2)$	(0.25±0.10)	(0.10±0.05)	0.50
$d(3-5)$	(2.40±0.10)	(2.41±0.08)	2.38
$d(1-3)$, $d(1-5)$	(2.34±0.10)		
$d(2-4)$, $d(2-6)$	(2.59±0.10)		
$d(6-4)$	(1.83±0.20)	(2.26±0.08)	2.37
$\Delta x(5-6)$, $\Delta x(3-4)$	(3.55±0.20)	(3.48±0.01)	
$d(7-9)$, $d(10-12)$	(2.43±0.10)	(2.38±0.02)	2.41
$\Delta x(7-8)$, $\Delta x(8-9)$, $\Delta x(10-11)$, $\Delta x(11-12)$	(3.40±0.20)	(3.43±0.01)	3.08
$d(3-10)$, $d(5-7)$	(2.22±0.10)		
$d(3-11)$, $d(5-8)$	(2.30±0.10)		
$d(4-11)$, $d(6-8)$	(2.35±0.10)		
$d(4-12)$, $d(6-9)$	(2.25±0.10)		
Δz(I−II)	(1.26±0.05)	(1.56±0.04)	
Δz(II−III)	(1.43±0.05)	(1.56±0.04)	
Δz(III−IV)	(0.89±0.05)		
Δz(IV−V)	(1.00±0.05)		
Δz(V−VI)	(1.09±0.05)		

shows clearly that these topmost reacted dimers are not broken upon hydrogen interaction.[26] Furthermore the general (3×2) surface ordering remains unchanged with no (3×1) transformation, even if the surface is reactive.[26] Therefore the reported (3×1) LEED structure[25] is not conclusive. One can rather interpret this observation by a defect-induced loss of $\times2$ long-range periodicity. Indeed, on the clean $3C$-SiC(001)$-(3\times2)$ surface, one observes the so-called "dimer-pair defect" and the correlated one-half unit cell parameter shift along the dimer row as evidenced by atom-resolved STM.[35] This type of defect leads to long anti-phase boundaries and is responsible for the long-range periodicity weakening along the $\times2$ direction.[35,39] Such an effect taking place on the clean surface may indeed be enhanced by atomic hydrogen interaction. Finally, one should also notice that a (3×1) LEED pattern has been observed to result from oxygen contamination of the $3C$-SiC(001)$-(3\times2)$ surface.[7]

V. CONCLUSIONS

In summary, we solve the atomic structure of the (3×2) reconstruction of cubic SiC(001) by using the photoelectron diffraction technique. We carry out bulk and surface sensitive experiments in angle-scanned mode to discriminate the model and determine the atomic positions of atoms in the three topmost layers. Multiple scattering calculations up to 11th order of scattering in a spherical wave formalism are carried out to simulate the experimental data. Specifically, we use C 1*s* and Si 2*p* azimuthal anisotropy curves excited with Mg K_α and their corresponding simulations to determine the bulk atomic positions. Si 2*p* azimuthal anisotropy curves at low photon energies allow us to settle the atomic structure of the $3C$-SiC(001)$-(3\times2)$ phase. The atomic structure found comprises the atomic positions of the three top atomic layers and the interlayer spacings of the top six atomic layers. We conclude that the (3×2) structure is well described by the alternating long and short dimer model (a modification of the TAADM-Si model), and that all other models proposed in the literature are not compatible with our results. We refine the ALSD-TAADM models using an *R*-factor minimization of the agreement between simulated and experimental azimuthal anisotropy curves at surface sensitive photon energies. The refinement leads to a corrugation of (0.25 ± 0.10) Å for the atoms in the outermost dimer. Atoms in the layer underneath dimerize as well, with alternating long and short bond lengths. The long-and-short alternateness between dimer bond lengths explains the top dimer asymmetry along one single direction. The dimerization takes place through lateral relaxation, without large vertical distortions. The third atomic layer is also dimerized, with a dimer bond length of (2.43 ± 0.10) Å. We conclude that our results, together with STM and GIXRD experimental techniques and theoretical calculations, converge in a unifying model for the $3C$-SiC(001)$-(3\times2)$ surface.

ACKNOWLEDGMENTS

This work was supported in part by MCyT (BFM2001-0244), MEyC (Secretaría de Estado de Educación y Universidades, PR2003-0030), and CAM (Spain) (07N/0022/2002 and FPI grant of A. Tejeda). The synchrotron radiation experiments performed at the ALS (Berkeley) have been supported by the Northern Illinois University Graduate School Funds and by NSF. F.J.G.A. acknowledges help and support from MCyT (MAT2001-0946) and UPV/EHU (00206.215-13639/2001). The authors are grateful to the ALS staff for expert and outstanding technical assistance.

*Present address: Department of Physics, University of Wisconsin Eau Claire, 105 Garfield Avenue, Eau Claire, Wisconsin 54701–4004, USA.

[1] *Silicon Carbide, A Review of Fundamental Questions and Applications to Current Device Technology*, edited by W. J. Choyke, H. M. Matsunami, and G. Pensl (Akademie Verlag, Berlin, 1998), Vols. I & II, and references therein.

[2] *Silicon Carbide Electronic Devices and Materials*, MRS Bull. **22** (1997), and references therein.

[3] *IEEE Transactions on Electron Devices*, special issue on Silicon Carbide Electronic Devices, **46** (3) (1999), and references therein.

[4] V. M. Bermudez, Phys. Status Solidi B **202**, 447 (1997), and references therein.

[5] P. Soukiassian, Mater. Sci. Eng., B **61**, 506 (1999), and references therein.

[6] M. Dayan, J. Vac. Sci. Technol. A **3**, 361 (1985).

[7] M. Dayan, J. Vac. Sci. Technol. A **4**, 38 (1986).

[8] R. Kaplan, Surf. Sci. **215**, 111 (1989).

[9] S. Hara, W. F. J. Slijkerman, J. F. van der Veen, I. Ohdomari, S. Misawa, E. Sakuma, and S. Yoshida, Surf. Sci. Lett. **231**, L196 (1990).

[10] T. Yoshinobu, I. Izumikawa, H. Mitsui, and T. Fuyuki, Appl. Phys. Lett. **59**, 2844 (1991).

[11] S. Hara, S. Misawa, S. Yoshida, and Y. Aoyagi, Phys. Rev. B **50**, 4548 (1994).

[12] V. M. Bermudez and J. P. Long, Appl. Phys. Lett. **66**, 475 (1995).

[13] S. Hara, J. Kitamura, H. Okushi, S. Misawa, S. Yoshida, and Y. Tokumaru, Surf. Sci. **357-358**, 436 (1996).

[14] F. Semond, L. Douillard, P. Soukiassian, D. Dunham, F. Amy, and S. Rivillon, Appl. Phys. Lett. **68**, 2144 (1996).

[15] F. Semond, P. Soukiassian, P. Mangat, Z. Hurych, L. di Cioccio, and C. Jaussaud, Appl. Surf. Sci. **104-105**, 79 (1996).

[16] H. W. Yeom, Y.-C. Chao, S. Terada, S. Hara, S. Yoshida, and R. I. G. Uhrberg, Phys. Rev. B **56**, R15525 (1997).

[17] H. W. Yeom, Y.-C. Chao, I. Matsuda, S. Hara, S. Yoshida, and R. I. G. Uhrberg, Phys. Rev. B **58**, 10540 (1998).

[18] M. Lübbe, K. Lindner, S. Sloboshanin, S. Tautz, J. Schäfer, and D. R.T. Zahn, J. Vac. Sci. Technol. A **16**, 3471 (1995).

[19] A. Mayne, F. Semond, G. Dujardin, and P. Soukiassian, Phys. Rev. B **57**, R15108 (1998).

[20] U. Rossow, K. Lindner, M. Lübbe, D. E. Aspnes, and D. R. T.

Zahn, J. Vac. Sci. Technol. B **16**, 2355 (1998).
[21] H. Nienhaus, V. van Elsbergen, and W. Mönch, Eur. Phys. J. B **9**, 179 (1999).
[22] J. Kitamura, S. Hara, H. Okushi, S. Yoshida, S. Misawa, and W. Kajimura, Surf. Sci. **433**, 465 (1999).
[23] S. Hara, J. Kitamura, H. Okushi, S. Misawa, S. Yoshida, K. Kajimura, H. W. Yeom, and R. I. G. Uhrberg, Surf. Sci. **421**, L143 (1999).
[24] H. W. Yeom, Y.-C. Chao, S. Terada, S. Hara, S. Yoshida, and R. I. G. Uhrberg, Surf. Sci. **433-435**, 392 (1999).
[25] H. W. Yeom, I. Matsuda, Y.-C. Chao, S. Hara, S. Yoshida, and R. I. G. Uhrberg, Phys. Rev. B **61**, R2417 (2000).
[26] V. Derycke, P. Soukiassian, F. Amy, Y. Chabal, M. D'angelo, H. Enriquez, and M. Silly, Nat. Mater. **2**, 263 (2003).
[27] M. Kitabatake and J. E. Greene, Jpn. J. Appl. Phys., Part 1 **35**, 5261 (1996).
[28] M. Kitabatake and J. E. Greene, Appl. Phys. Lett. **69**, 2048 (1996).
[29] W. Lu, W. G. Schmidt, E. L. Briggs, and J. Bernholc, Phys. Rev. Lett. **85**, 4381 (2000).
[30] H. Yan, A. P. Smith, and H. Jónsson, Surf. Sci. **330**, 265 (1995).
[31] W. Lu, P. Krüger, and J. Pollmann, Phys. Rev. B **60**, 2495 (1999).
[32] S. A. Shevlin and A. J. Fisher, Appl. Surf. Sci. **162-163**, 94 (2000).
[33] L. Pizzagalli, A. Catellani, G. Galli, F. Gygi, and A. Baratoff, Phys. Rev. B **60**, R5129 (1999).
[34] V. M. Bermudez, in Ref. 1, p. 447.
[35] F. Semond, P. Soukiassian, A. Mayne, G. Dujardin, L. Douillard, and C. Jaussaud, Phys. Rev. Lett. **77**, 2013 (1996).
[36] P. Soukiassian, F. Semond, A. Mayne, and G. Dujardin, Phys. Rev. Lett. **79**, 2498 (1997).
[37] L. Douillard, V. Yu. Aristov, F. Semond, and P. Soukiassian, Surf. Sci. **401**, L395 (1998).
[38] V. Yu. Aristov, L. Douillard, and P. Soukiassian, Surf. Sci. **440**, L825 (1999).
[39] M. D'angelo, H. Enriquez, V. Yu. Aristov, P. Soukiassian, G. Renaud, A. Barbier, M. Noblet, S. Chiang, and F. Semond, Phys. Rev. B **68**, 165321 (2003).
[40] W. F. Egelhoff, Crit. Rev. Solid State Mater. Sci. **16**, 213 (1990).
[41] C. S. Fadley, M. A. Van Hove, Z. Hussain, A. P. Kaduwela, R. E. Couch, Y. J. Kim, P. M. Len, J. Palomares, S. Ryce, S. Ruebush, E. D. Tober, Z. Wang, R. X. Ynzunza, H. Daimon, H. Galloway, M. B. Salmeron, and W. Schattke, Surf. Rev. Lett. **4**, 421 (1997).
[42] A. Mascaraque, J. Avila, C. Teodorescu, M. C. Asensio, and E. G. Michel, Phys. Rev. B **55**, R7315 (1997).
[43] E. L. Bullock, G. S. Herman, M. Yamada, D. J. Friedman, and C. S. Fadley, Phys. Rev. B **41**, 1703 (1990).
[44] R. Terborg, P. Baumgärtel, R. Lindsay, O. Schaff, T. Gießel, J. T. Hoeft, M. Polcik, R. L. Toomes, S. Kulkarni, A. M. Bradshaw, and D. P. Woodruff, Phys. Rev. B **61**, 16697 (2000).
[45] E. L. Bullock, R. Gunnella, L. Patthey, T. Abukawa, S. Kono, C. R. Natoli, and L. S.O. Johansson, Phys. Rev. Lett. **74**, 2756 (1995).
[46] M. Shimomura, T. Abukawa, K. Yoshimura, J. H. Oh, H. W. Yeom, and S. Kono, Surf. Sci. **493**, 23 (2001).
[47] S. A. Chambers, S. B. Anderson, and J. H. Weaver, Phys. Rev. B **32**, 581 (1985).
[48] S. W. King, C. Ronning, R. F. Davis, R. S. Busby, and R. J. Nemanich, J. Appl. Phys. **84**, 6042 (1998).
[49] L. Simon, J. L. Bischoff, and L. Kubler, Phys. Rev. B **60**, 11653 (1999).
[50] O. M. Küttel, R. G. Agostino, R. Fasel, J. Osterwalder, and L. Schlapbach, Surf. Sci. **312**, 131 (1994).
[51] C. Pirri, M. H. Tuilier, P. Wetzel, S. Hong, D. Bolmont, G. Gewinner, R. Cortès, O. Heckmann, and H. von Känel, Phys. Rev. B **51**, 2302 (1995).
[52] S. Kono, J. Electron Spectrosc. Relat. Phenom. **126**, 43 (2002), and references therein.
[53] M. Shimomura, H. W. Yeom, B. S. Mun, C. S. Fadley, S. Hara, S. Yoshida, and S. Kono, Surf. Sci. **438**, 237 (1999).
[54] Y. Chen, F. J. García de Abajo, A. Chassé, R. X. Ynzunza, A. P. Kaduwela, M. A. Van Hove, and C. S. Fadley, Phys. Rev. B **58**, 13121 (1998); Y. Chen and M. A. Van Hove, http://electron.lbl.gov/mscdpack/.
[55] F. J. García de Abajo, M. A. Van Hove, and C. S. Fadley, Phys. Rev. B **63**, 075404 (2001). See also EDAC code at http://electron.lbl.gov/edac and http://dipc.ehu.es/edac.
[56] The mean free path was calculated according to Ref. 57. During the refinement of low kinetic energy data, the mean free path was fitted as a parameter (optimum value: 3 Å).
[57] S. Tanuma, C. J. Powell, and D. R. Penn, Surf. Interface Anal. **17**, 927 (1991).
[58] The domains considered are due to the fact that a 180° rotation of the whole cluster shown in Fig. 10 is an equally acceptable structure. This domain structure does not affect the LEED pattern.
[59] R. S. Saiki, A. P. Kaduwela, M. Sagurton, J. Osterwalder, D. J. Friedman, C. S. Fadley, and C. R. Brundle, Surf. Sci. **282**, 33 (1993).
[60] M. A. Van Hove, S. Y. Tong, and M. H. Elconin, Surf. Sci. **64**, 85 (1977).
[61] High kinetic energy peaks are mostly sensitive to interatomic directions in the bulk. However, they are also affected by other factors as the surface structure itself. A more accurate fit would require one to optimize the structure of the surface layer, as is done in the refinement process.
[62] R. Fasel, P. Aebi, J. Osterwalder, L. Schlapbach, R. G. Agostino, and G. Chiarello. Phys. Rev. B **50**, 14516 (1994).
[63] The *R*-factor in this paper is calculated without smoothing. It is known that smoothing leads to a markedly lower *R*-factor value (Ref. 64).
[64] M. Van Hove, W. Moritz, H. Over, P. J. Rous, A. Wander, A. Barbieri, N. Materer, U. Starke, and G. A. Somorjai, Surf. Sci. Rep. **19**, 191 (1993).
[65] We found a position of the surface of $z_0 = 2.25$ Å. The inner potential was optimized for each energy, with values in the range 5–15 eV. See also Ref. 56.
[66] M. Takahashi, S. Nakatani, Y. Ito, T. Takahashi, X. W. Zhang, and M. Ando, Surf. Sci. **357-358**, 78 (1996).
[67] J. J. Boland, Phys. Rev. Lett. **65**, 3325 (1990); **67**, 1539 (1991); Surf. Sci. **261**, 17 (1992).